

Graphene Ambipolar Nanoelectronics for High Noise Rejection Amplification

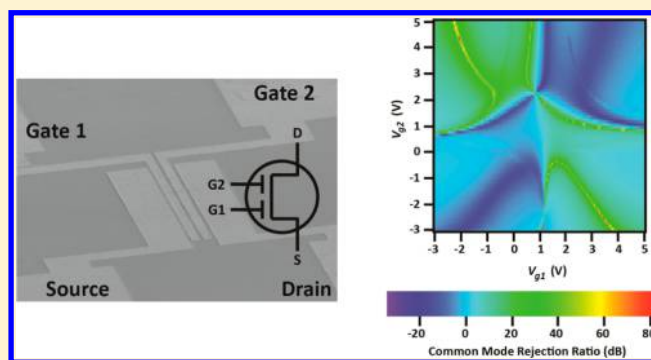
Che-Hung Liu, Qi Chen, Chang-Hua Liu, and Zhaohui Zhong*

Department of Electrical Engineering and Computer Science, University of Michigan, Ann Arbor, Michigan 48109, United States

S Supporting Information

ABSTRACT: In a modern wireless communication system, signal amplification is critical for overcoming losses during multiple data transformations/processes and long-distance transmission. Common mode and differential mode are two fundamental amplification mechanisms, and they utilize totally different circuit configurations. In this paper, we report a new type of dual-gate graphene ambipolar device with capability of operating under both common and differential modes to realize signal amplification. The signal goes through two stages of modulation where the phase of signal can be individually modulated to be either in-phase or out-of-phase at two stages by exploiting the ambipolarity of graphene. As a result, both common and differential mode amplifications can be achieved within one single device, which is not possible in the conventional circuit configuration. In addition, a common-mode rejection ratio as high as 80 dB can be achieved, making it possible for low noise circuit application. These results open up new directions of graphene-based ambipolar electronics that greatly simplify the RF circuit complexity and the design of multifunction device operation.

KEYWORDS: Graphene, ambipolar, nanoelectronics, amplification, wireless communication system



With over half of the world's population having access to cellular phones and other mobile/wearable information devices, there is a definite movement toward the realization of ubiquitously available wireless communication system that are even more compact and portable. Among the wireless communication system, signal amplification is one of the key processes for overcoming losses during multiple data transformations and long-distance transmission. There are four basic types of electronic amplifiers: voltage, current, transconductance, and transresistance amplifiers.¹ Generally, the voltage amplifier is the most common one and widely used in modern circuit architecture. More specifically, there are two main kinds of amplification mechanisms for voltage amplifiers, that is, common and differential mode amplifications, respectively.² Common mode is basically the most generic concept of amplification, which amplifies particular input signal, while the differential mode amplifies the voltage difference between two input signals. Both the common and differential mode amplifiers are crucial and widely used in the circuitry nowadays, however, they utilize two totally different circuit configurations.

During the past decade, graphene has been widely studied and has shown extremely high intrinsic carrier mobility at room temperature,^{3–5} linear dispersion relation in energy band structure, and ambipolar behavior for both electron- and hole-dominated regions.^{6–8} In particular, the intriguing ambipolarity of graphene has enabled unique RF device applications^{9,10} which not only provide greater controllability

for signal processing and modulation but with much simplified circuitry. Recent advances in graphene-integrated electronics have led to notable progress: a number of RF integrated circuits with various functionality have been successfully demonstrated including mixer,^{11–14} frequency doubler,^{15,16} tripler,¹⁷ multiplier,^{18,19} antenna,^{20–22} and receiver.²³ Moreover, researchers also achieved circuit logic operation,²⁴ inverter,^{25–27} modulator^{28,29} and electromechanical devices, such as resonators^{30,31} and switch.³² Flexible and transparent graphene-based device and circuit were also demonstrated,^{28,33–35} which further showcase the possibilities of graphene for novel nanoelectronic applications.

In this paper, we report an extremely simple device design that can be programmed to achieve the functionality of both common and differential mode amplifications. We designed and fabricated a new type of dual-gate graphene ambipolar device, where the phase of the RF signal can be modulated independently at two gates to be either in phase or out of phase. This unusual tunability is enabled by the unique ambipolarity of graphene and leads to both common mode and differential mode operations in a single device. In addition, these devices can achieve a common-mode rejection ratio

Received: October 15, 2015

Revised: January 21, 2016

Published: January 25, 2016

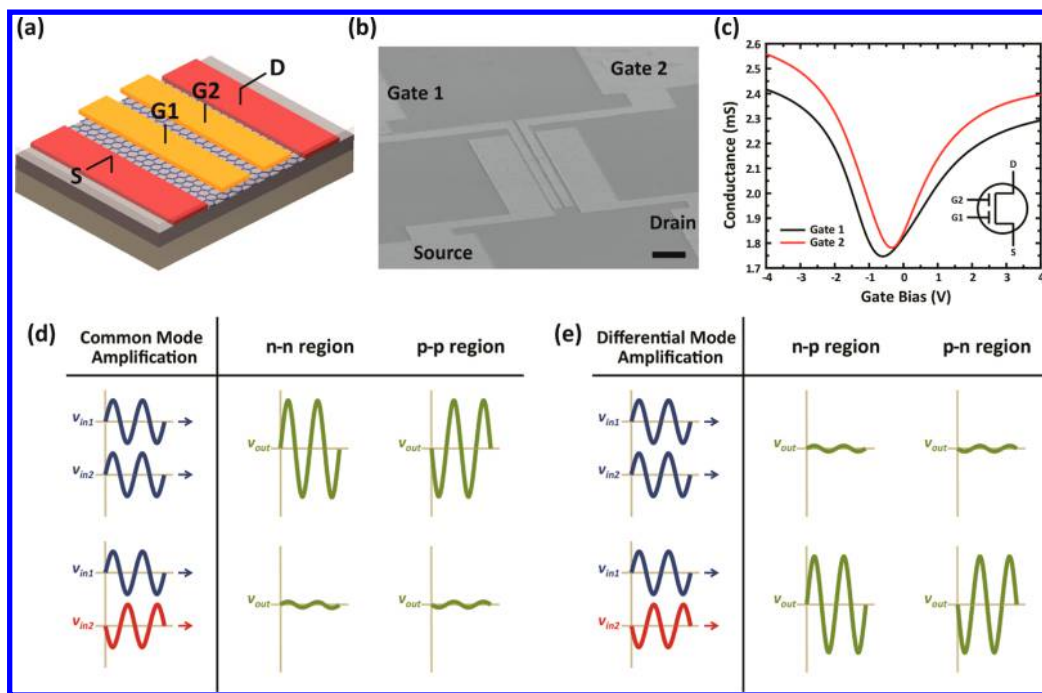


Figure 1. Device geometry of dual-gate graphene ambipolar device and its operation mechanism. (a) Schematic of the device. Source (S) and drain (D) electrodes are shown in red, and the dual-gate electrodes (G1 and G2) are shown in yellow. (b) The SEM image of the fabricated device. Scale bar, 10 μm . (c) The conductance versus gate voltage response curves for gate 1 (black) and gate 2 (red). The inset illustrates the proposed equivalent circuit symbol of our dual-gate graphene ambipolar device. (d) Schematic showing the common mode operation mechanism. Two ac inputs (v_{in1} and v_{in2}) are supplied through two gates, and the output signal (v_{out}) is recorded at the drain of the device with source grounded. (e) Schematic showing the differential mode operation mechanism.

(CMRR) as high as 80 dB, making it relevant for low noise circuit applications.

Figure 1a shows the schematic of dual-gate graphene ambipolar device structure and the scanning electron microscope (SEM) image of the actual fabricated device is shown in Figure 1b. Briefly, a monolayer graphene film grown by chemical vapor deposition (CVD) is transferred and patterned into transistor channel, and two electrostatically coupled metal gates, deposited after drain-source metal and dielectric layer, provide modulation to the RF signal (Supporting Information S1). During a typical operation, drain-source is dc biased with a supplied voltage, and two gates are dc biased at the desired biasing points. The ac input is supplied through two gates via bias tees, and the output signal is recorded at the drain with a ac lock-in amplifier and oscilloscope. The conductance-gate voltage transfer curves for two independent gates are shown in Figure 1c, where the ambipolarity is clearly presented with Dirac points at -0.6 and -0.34 V for gate 1 and 2, respectively. The carrier mobility can be extracted by fitting the transistor transfer curves,^{28,36} and the device presented in Figure 1c has a hole mobility of $844\text{ cm}^2\text{ V}^{-1}\text{ s}^{-1}$ and electron mobility of $866\text{ cm}^2\text{ V}^{-1}\text{ s}^{-1}$ (Supporting Information S2). Here, both gate 1 and 2 offer electrostatic control of electron-dominated versus hole-dominated transport within graphene channel (Supporting Information Figure S1). We propose a new equivalent circuit symbol, shown in Figure 1c inset, for our ambipolar device to represent in dual gate tuning.

Next, we examine how independent modulation by the two gates can be configured to achieve common and differential mode operations. The key principle lies in the ambipolarity of graphene: the phase of an ac input can be shifted by 180° when

switching the dc gate biasing point from electron-dominated region to hole-dominated region, and vice versa.²⁸

To achieve common mode operation, one can configure the phase modulation of gate 1 and 2 to be in phase by dc biasing two gates in the same electron- (or hole-) dominated region (Figure 1d). As shown in the schematic, two in-phase input signals are amplified with the same phase, which lead to two in-phase outputs and add up to a significant overall output signal. On the other hand, two out-of-phase input signals yield two out-of-phase outputs, which cancel each other and lead to a negligible overall output signal. As the result, the dual-gate graphene ambipolar device is functioning as a common-mode amplifier.

For differential mode operations, one can configure the phase modulation of gate 1 and 2 to be out-of-phase (n-p or p-n region) by dc biasing one gate in electron-dominated region, and the other gate in hole-dominated region (Figure 1e). Contrary to the common mode operation, two out-of-phase input signals are amplified with opposite phase, which lead to two in-phase outputs and add up to a significant overall output signal. On the other hand, two in-phase input signals yield two out-of-phase outputs, which cancel each other and lead to a negligible overall output signal. As the result, the dual-gate graphene ambipolar device is configured as a differential mode amplifier by simply changing the gate biasing conditions. We note that one can also operate one of the gates at the charge-neutral Dirac point, and the device will become a typical graphene transistor.

To experimentally verify the common mode operation, we test our dual-gate graphene ambipolar device with two in-phase ac inputs. Figure 2a shows the electrical measurement setup. Here, we use the built-in sinusoidal wave generated from the

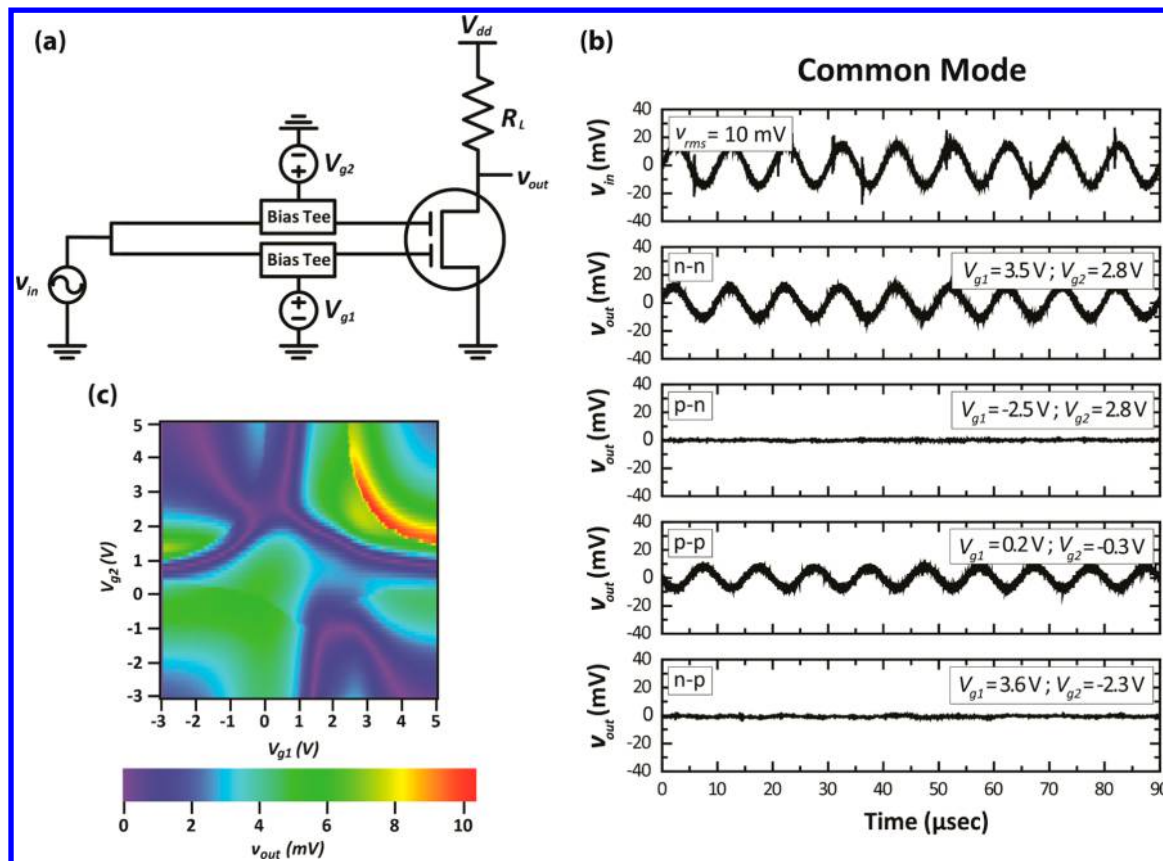


Figure 2. Common mode operation demonstrated by the dual-gate graphene ambipolar device. (a) Diagram of the electrical measurement setup. $R_L = 0.5$ kohm and $V_{dd} = 10$ V. (b) The time-traced ac voltage amplitude curves recorded for input and the outputs under n–n, p–n, p–p, and n–p dual-gate biasing conditions. (c) Two-dimensional color plot of output voltage amplitude versus the dual-gate biasing voltages. In–phase ac inputs ($v_{in} = 10$ mV) are supplied at two gates during the measurement for common mode operation.

lock-in amplifier (Stanford Research Systems SR830) as our ac source ($v_{ac} = 10$ mV, $f = 100$ kHz), which is coupled into two gates through bias tees for the two ac inputs. The output signal is measured at the drain using the lock-in amplifier with source grounded. Four different gate biasing conditions are tested, which are n–n ($V_{g1} = 3.5$ V, $V_{g2} = 2.8$ V), p–p ($V_{g1} = 0.2$ V, $V_{g2} = -0.3$ V), p–n ($V_{g1} = -2.5$ V, $V_{g2} = 2.8$ V), and n–p ($V_{g1} = 3.6$ V, $V_{g2} = -2.3$ V) regions. Figure 2b shows real-time output signal waveform under these four gate biasing conditions, together with the input waveform. When two gates are biased in the same electron-dominated (n–n) or hole-dominated (p–p) region, we recover the sinusoidal waveform at the output. On the contrary, when two gates are biased in p–n or n–p region, the output signal amplitude is negligible. These results confirm the common mode operation mechanism illustrated in Figure 1d. Furthermore, in order to present the complete picture of how dual-gate graphene ambipolar device response to two in-phase inputs, we measure the output signal amplitude when sweeping both gates across the Dirac point (Figure 2c). As shown in the two-dimensional color plot, the output signals in n–n and p–p regions are significantly larger than the signals in p–n and n–p regions. The maximum achievable common mode gain is larger than unity under corresponding gate biasing point in n–n region. We note that the slight difference in n–n and p–p regions is caused by the asymmetry of electron and hole transport.

We also examine the differential mode operation by testing the same dual-gate graphene ambipolar device with two out-of-

phase inputs. Here, we use a phase shift circuit (Supporting Information Figure S2) in one of the gates in order to achieve 180° phase difference between two inputs (Figure 3a). We again tested four different gate biasing conditions, which are n–n ($V_{g1} = 2.5$ V, $V_{g2} = 3.4$ V), p–n ($V_{g1} = -0.8$ V, $V_{g2} = 3.2$ V), p–p ($V_{g1} = -0.5$ V, $V_{g2} = -0.3$ V), and n–p ($V_{g1} = 2.4$ V, $V_{g2} = 0.5$ V). As shown in Figure 3b, we recover a strong sinusoidal waveform at the output when two gates are biased in p–n or n–p regions. On the contrary, when two gates are biased in n–n or p–p region, the output signal amplitude is negligible. These results contrast the common mode operation shown earlier, and confirm the differential mode operation mechanism illustrated in Figure 1e. A more complete picture is shown in Figure 3c, where the output signal amplitude is again plotted against two gate biasing voltages. Noticeably, large output signal regions are located in n–p or p–n regions, which is the exact opposite of the common mode operation scenario shown in Figure 2c. Furthermore, a voltage gain higher than 1.7 is obtained under differential mode operation.

With the results from both common and differential mode operations, we can further calculate the common mode rejection ratio (CMRR) given by

$$\text{CMRR} = 20 \log_{10} \left(\frac{A_d}{|A_c|} \right) \text{dB}$$

where A_d and A_c are the amplification gain for differential and common mode operation. The calculated two-dimensional CMRR at varying gate biasing voltages is shown in Figure 4.

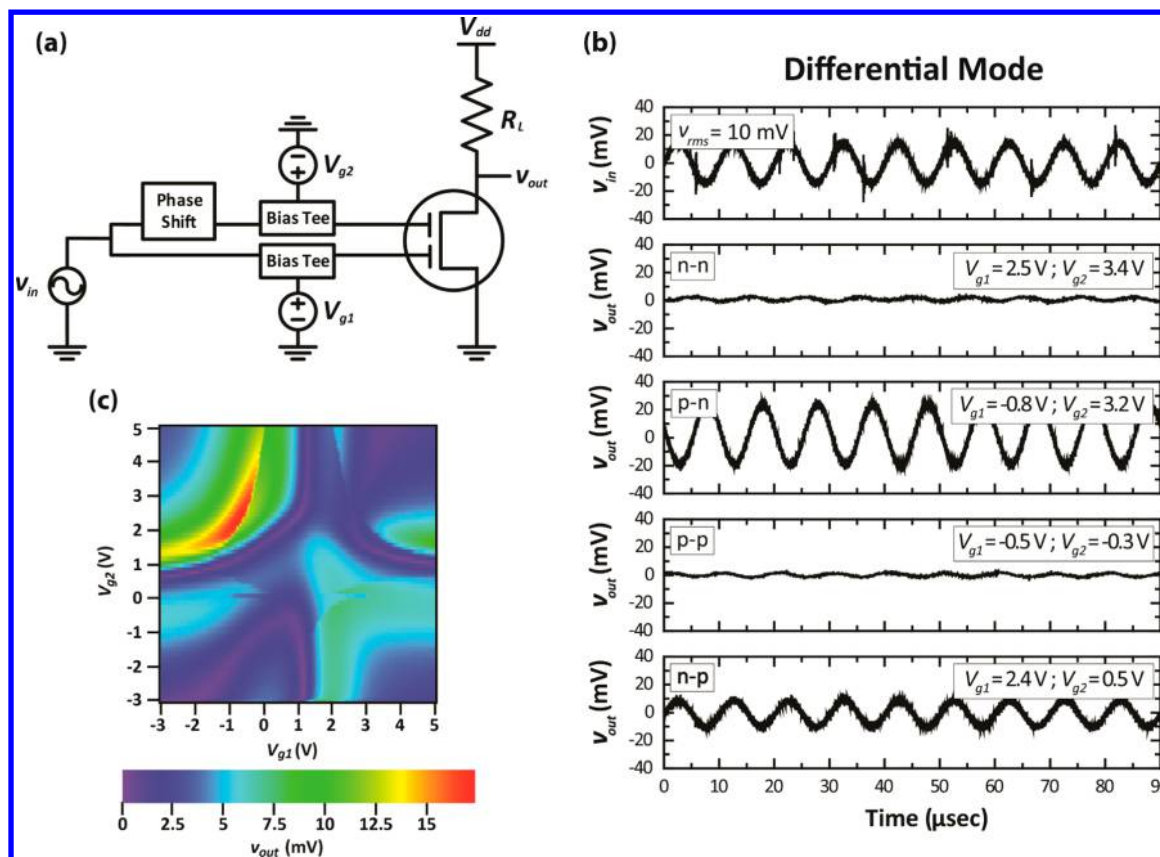


Figure 3. Differential mode operation demonstrated by the dual-gate graphene ambipolar device. (a) Diagram of the electrical measurement setup. $R_L = 0.5$ kohm and $V_{dd} = 10$ V. A phase shift circuit is used in one of the gates in order to achieve 180° phase difference between two inputs. (b) The time-traced ac voltage amplitude curves recorded for input and outputs under n–n, p–n, p–p, and n–p dual-gate biasing conditions. (c) Two-dimensional color plot of output voltage amplitude versus the dual-gate biasing voltages. Out-of-phase ac inputs ($v_{in} = 10$ mV) are supplied at two gates during the measurement for differential mode operation.

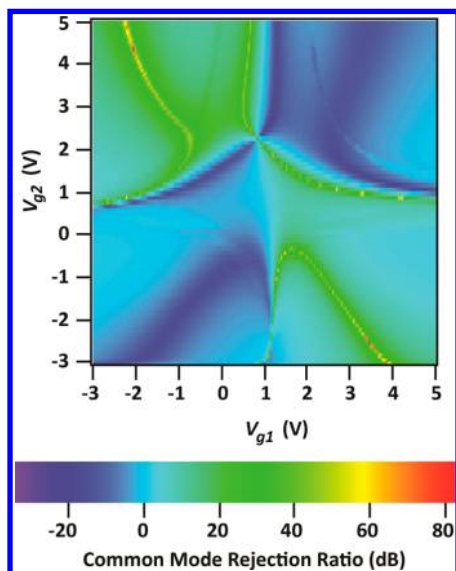


Figure 4. Two-dimensional color plot of common mode rejection ratio versus the dual-gate biasing voltages. The CMRR values are calculated from the common mode and differential mode measurements plotted in Figures 2c and 3c. High noise rejection can be achieved with either p–n or n–p differential mode biasing conditions.

From the plot, we observe under appropriate gate biasing points that our unoptimized dual-gate graphene ambipolar

device can already achieve CMRR of over 80 dB. Importantly, our device utilizes a much simplified design compared to conventional amplifier, namely a single device can achieve both common and differential mode amplifications. We note that all measured devices show the same characteristics and confirm the high CMRR (Supporting Information Figure S3). In addition, our device shows a clean spectrum and higher order harmonics are negligible (Supporting Information Figure S4).

In summary, we demonstrated a new type of dual-gate graphene ambipolar device that can be configured as both common mode and differential mode amplifiers. Compared to conventional silicon-based amplifiers, our design consists of one single graphene device yet can achieve CMRR of over 80 dB. Our current generation of devices is not without some serious limitations. First, the lack of current saturation (Supporting Information Figure S5) due to the semimetallic nature of graphene, potentially limits the intrinsic voltage gain and maximum frequency of the devices. Second, the device is still limited by the small voltage gain, ~ 1 for common mode operation and close to 2 for differential mode operation. However, high gain graphene amplifiers have been shown in literatures through the adoption of high- k dielectrics³⁷ and thinner dielectrics.³⁸ More importantly, the results shown here hint at a broad range of graphene-based ambipolar electronics which can enable More-Moore and More-than-Moore technologies^{39–42} in the post-CMOS era.

■ ASSOCIATED CONTENT

📄 Supporting Information

The Supporting Information is available free of charge on the ACS Publications website at DOI: 10.1021/acs.nanolett.5b04203.

(Additional information includes materials and device fabrication, carrier mobility extraction, two-dimensional conductance color plot versus dual-gate biasing voltages, circuit diagram for the home-built phase shift module, and two-dimensional CMRR measurements on two other devices. PDF)

■ AUTHOR INFORMATION

Corresponding Author

*E-mail: zzhong@umich.edu.

Author Contributions

The manuscript was written through contributions of all authors. All authors have given approval to the final version of the manuscript.

Notes

The authors declare no competing financial interest.

■ ACKNOWLEDGMENTS

This work was supported by National Science Foundation Scalable Nanomanufacturing Program (DMR-1120187) and CAREER Award (ECCS-1254468). The devices were fabricated and characterized at the Lurie Nanofabrication Facility at the University of Michigan, a member of the National Nanotechnology Infrastructure Network funded by the National Science Foundation.

■ REFERENCES

- (1) Sedra, A. S.; Smith, K. C. *Microelectronic Circuits*; Oxford University Press: New York, 2007.
- (2) Razavi, B. *Design of Analog CMOS Integrated Circuits*; McGraw-Hill: New York, 2001.
- (3) Chen, J.-H.; Jang, C.; Xiao, S.; Ishigami, M.; Fuhrer, M. S. *Nat. Nanotechnol.* **2008**, *3* (4), 206–209.
- (4) Bolotin, K. I.; Sikes, K. J.; Jiang, Z.; Klima, M.; Fudenberg, G.; Hone, J.; Kim, P.; Stormer, H. L. *Solid State Commun.* **2008**, *146* (9–10), 351–355.
- (5) Morozov, S. V.; Novoselov, K. S.; Katsnelson, M. I.; Schedin, F.; Elias, D. C.; Jaszczak, J. A.; Geim, A. K. *Phys. Rev. Lett.* **2008**, *100* (1), 016602.
- (6) Novoselov, K. S.; Geim, A. K.; Morozov, S. V.; Jiang, D.; Zhang, Y.; Dubonos, S. V.; Grigorieva, I. V.; Firsov, A. A. *Science* **2004**, *306* (5696), 666–669.
- (7) Zhang, Y.; Tan, Y.-W.; Stormer, H. L.; Kim, P. *Nature* **2005**, *438* (7065), 201–204.
- (8) Novoselov, K. S.; Geim, A. K.; Morozov, S. V.; Jiang, D.; Katsnelson, M. I.; Grigorieva, I. V.; Dubonos, S. V.; Firsov, A. A. *Nature* **2005**, *438* (7065), 197–200.
- (9) Palacios, T.; Hsu, A.; Wang, H. *IEEE Commun. Mag.* **2010**, *48* (6), 122–128.
- (10) Lee, S.; Zhong, Z. *Nanoscale* **2014**, *6* (22), 13283–13300.
- (11) Wang, H.; Hsu, A.; Wu, J.; Kong, J.; Palacios, T. *IEEE Electron Device Lett.* **2010**, *31* (9), 906–908.
- (12) Madan, H.; Hollander, M. J.; LaBella, M.; Cavalero, R.; Snyder, D.; Robinson, J. A.; Datta, S. In *Electron Devices Meeting (IEDM), 2012 IEEE International*; 2012; pp 4.3.1–4.3.4.
- (13) Habibpour, O.; Vukusic, J.; Stake, J. *IEEE Trans. Microwave Theory Tech.* **2013**, *61* (2), 841–847.

(14) Moon, J. S.; Seo, H.-C.; Antcliffe, M.; Le, D.; McGuire, C.; Schmitz, A.; Nyakiti, L. O.; Gaskill, D. K.; Campbell, P. M.; Lee, K.-M.; Asbeck, P. *IEEE Electron Device Lett.* **2013**, *34* (3), 465–467.

(15) Wang, Z.; Zhang, Z.; Xu, H.; Ding, L.; Wang, S.; Peng, L.-M. *Appl. Phys. Lett.* **2010**, *96* (17), 173104.

(16) Ramon, M. E.; Parrish, K. N.; Lee, J.; Magnuson, C. W.; Tao, L.; Ruoff, R. S.; Banerjee, S. K.; Akinwande, D. *IEEE Int. Electron Devices Meet.* **2012**, 1–3.

(17) Chen, H.-Y.; Appenzeller, J. *Nano Lett.* **2012**, *12* (4), 2067–2070.

(18) Wang, H.; Nezich, D.; Kong, J.; Palacios, T. *IEEE Electron Device Lett.* **2009**, *30* (5), 547–549.

(19) Wang, H.; Hsu, A.; Kim, K. K.; Kong, J.; Palacios, T. *IEEE Int. Electron Devices Meet.* **2010**, 23.6.1–23.6.4.

(20) Dragoman, M.; Muller, A. A.; Dragoman, D.; Coccetti, F.; Plana, R. *J. Appl. Phys.* **2010**, *107* (10), 104313.

(21) Tamagnone, M.; Gómez-Díaz, J. S.; Mosig, J. R.; Perruisseau-Carrier, J. *Appl. Phys. Lett.* **2012**, *101* (21), 214102.

(22) Alarcón, E.; Chigrin, D. N. *Photonics Nanostructures - Fundam. Appl.* **2012**, *10* (4), 353–358.

(23) Han, S.-J.; Garcia, A. V.; Oida, S.; Jenkins, K. A.; Haensch, W. *Nat. Commun.* **2014**, *5*, 3086.

(24) Sordan, R.; Traversi, F.; Russo, V. *Appl. Phys. Lett.* **2009**, *94* (7), 073305.

(25) Traversi, F.; Russo, V.; Sordan, R. *Appl. Phys. Lett.* **2009**, *94* (22), 223312.

(26) Harada, N.; Yagi, K.; Sato, S.; Yokoyama, N. *Appl. Phys. Lett.* **2010**, *96* (1), 012102.

(27) Li, S.-L.; Miyazaki, H.; Kumatani, A.; Kanda, A.; Tsukagoshi, K. *Nano Lett.* **2010**, *10* (7), 2357–2362.

(28) Lee, S.; Lee, K.; Liu, C.-H.; Kulkarni, G. S.; Zhong, Z. *Nat. Commun.* **2012**, *3*, 1018.

(29) Sensale-Rodriguez, B.; Yan, R.; Kelly, M. M.; Fang, T.; Tahy, K.; Hwang, W. S.; Jena, D.; Liu, L.; Xing, H. G. *Nat. Commun.* **2012**, *3*, 780.

(30) Bunch, J. S.; Zande, A. M. van der; Verbridge, S. S.; Frank, I. W.; Tanenbaum, D. M.; Parpia, J. M.; Craighead, H. G.; McEuen, P. L. *Science* **2007**, *315* (5811), 490–493.

(31) Chen, C.; Rosenblatt, S.; Bolotin, K. I.; Kalb, W.; Kim, P.; Kymissis, I.; Stormer, H. L.; Heinz, T. F.; Hone, J. *Nat. Nanotechnol.* **2009**, *4* (12), 861–867.

(32) Milaninia, K. M.; Baldo, M. A.; Reina, A.; Kong, J. *Appl. Phys. Lett.* **2009**, *95* (18), 183105.

(33) Bae, S.; Kim, H.; Lee, Y.; Xu, X.; Park, J.-S.; Zheng, Y.; Balakrishnan, J.; Lei, T.; Ri Kim, H.; Song, Y. I.; Kim, Y.-J.; Kim, K. S.; Özyilmaz, B.; Ahn, J.-H.; Hong, B. H.; Iijima, S. *Nat. Nanotechnol.* **2010**, *5* (8), 574–578.

(34) Lin, Y.-M.; Valdes-Garcia, A.; Han, S.-J.; Farmer, D. B.; Meric, I.; Sun, Y.; Wu, Y.; Dimitrakopoulos, C.; Grill, A.; Avouris, P.; Jenkins, K. A. *Science* **2011**, *332* (6035), 1294–1297.

(35) Georgiou, T.; Jalil, R.; Belle, B. D.; Britnell, L.; Gorbachev, R. V.; Morozov, S. V.; Kim, Y.-J.; Gholinia, A.; Haigh, S. J.; Makarovskiy, O.; Eaves, L.; Ponomarenko, L. A.; Geim, A. K.; Novoselov, K. S.; Mishchenko, A. *Nat. Nanotechnol.* **2012**, *8* (2), 100–103.

(36) Kim, S.; Nah, J.; Jo, I.; Shahrjerdi, D.; Colombo, L.; Yao, Z.; Tutuc, E.; Banerjee, S. K. *Appl. Phys. Lett.* **2009**, *94* (6), 062107.

(37) Han, S.-J.; Jenkins, K. A.; Valdes Garcia, A.; Franklin, A. D.; Bol, A. A.; Haensch, W. *Nano Lett.* **2011**, *11* (9), 3690–3693.

(38) Andersson, M. A.; Habibpour, O.; Vukusic, J.; Stake, J. *Electron. Lett.* **2012**, *48* (14), 861–863.

(39) Van Noorden, R. *Nature* **2006**, *442* (7100), 228–229.

(40) Taghioskoui, M. *Mater. Today* **2009**, *12* (10), 34–37.

(41) Cavin, R. K.; Lugli, P.; Zhirnov, V. V. *Proc. IEEE* **2012**, *100* (Special Centennial Issue), 1720–1749.

(42) Wu, J.; Shen, Y.-L.; Reinhardt, K.; Szu, H.; Dong, B. *Appl. Comp. Intell. Soft Comput.* **2013**, *2013*, 1–13.